Mechanism and Function of Mixed-Mode Oscillations in Vibrissa Motoneurons

David Golomb*

Departments of Physiology and Cell Biology, Physics and Zlotowski Center for Neuroscience, Faculty of Health Sciences, Ben Gurion University, Be'er-Sheva, Israel

Abstract

Vibrissa motoneurons in the facial nucleus innervate the intrinsic and extrinsic muscles that move the whiskers. Their intrinsic properties affect the way they process fast synaptic input from the vIRT and Bötzinger nuclei together with serotonergic neuromodulation. In response to constant current (I_{app}) injection, vibrissa motoneurons may respond with mixed mode oscillations (MMOs), in which sub-threshold oscillations (STOs) are intermittently mixed with spikes. This study investigates the mechanisms involved in generating MMOs in vibrissa motoneurons and their function in motor control. It presents a conductance-based model that includes the M-type K$^+$ conductance, g_M, the persistent Na$^+$ conductance, g_{NaP}, and the cationic h conductance, g_h. For $g_h = 0$ and moderate values of g_M and g_{NaP}, the model neuron generates STOs, but not MMOs, in response to I_{app} injection. STOs transform abruptly to tonic spiking as the current increases. In addition to STOs, MMOs are generated for $g_h > 0$ for larger values of I_{app}; the I_{app} range in which MMOs appear increases linearly with g_h. In the MMOs regime, the firing rate increases with I_{app} like a Devil's staircase. Stochastic noise disrupts the temporal structure of the MMOs, but for a moderate noise level, the coefficient of variation (CV) is much less than one and varies non-monotonically with I_{app}. Furthermore, the estimated time period between voltage peaks, based on Bernoulli process statistics, is much higher in the MMOs regime than in the tonic regime. These two phenomena do not appear when moderate noise generates MMOs without an intrinsic MMO mechanism. Therefore, and since STOs do not appear in spinal motoneurons, the analysis can be used to differentiate different MMOs mechanisms. MMO firing activity in vibrissa motoneurons suggests a scenario in which moderate periodic inputs from the vIRT and Bötzinger nuclei control whisking frequency, whereas serotonergic neuromodulation controls whisking amplitude.

Introduction

Motoneurons in the facial nucleus [1] innervate the intrinsic and extrinsic muscles that move the whiskers of rodents [2–6]. The frequency range of exploratory whisking in rats is 5–15 Hz [4], and the firing rate of vibrissa motoneurons can be as low as a few Hz [7,8]. These motoneurons are not mutually coupled, and are innervated by many brainstem areas [9]. Motoneurons that project to intrinsic and extrinsic muscles receive rhythmic synaptic input from the vIRT and Bötzinger nuclei respectively [10,11], and both types of motoneurons are under the modulation of serotonin and other neuromodulators [8,12]. It is still unclear how those inputs are integrated, or the ways in which integration is affected by the intrinsic properties of vibrissa motoneurons.

Intrinsic neuronal properties are often examined in *in vitro* experiments. Like other neurons, vibrissa motoneurons fire tonically under the application of applied current I_{app} if I_{app} is above a critical value. Below this value, they may fire in mixed mode oscillations (MMOs) [13], an alternation of subthreshold oscillations (STOs) with spiking behavior (Figure 3A in [12] and Figure 5A in [14]). At first glance, the inter-spike interval during these MMO states appears irregular. From an ionic current perspective, the firing of vibrissa motoneurons depends strongly on

the level of the persistent Na$^+$ conductance g_{NaP} [8], and enhancing g_{NaP} by a serotonergic agonist generates rhythmic firing in vibrissa motoneurons. Spiking in vibrissa motoneurons is followed by pronounced afterhyperpolarization, and the low firing rate is explained by AHP conductances that are significantly slower than AHP conductances in spinal motoneurons [8,15]. These neurons also exhibit an h-conductance and response in that they "sag" to hyperpolarizing current steps [16].

In addition to rat vibrissa motoneurons, MMOs have been found in mouse [17] and rat [18] spinal motoneurons. In spinal motoneurons, the firing frequency in the tonic regime ("primary range"), as well as the frequency of the STOs between spikes in the MMO regime ("sub-primary range) were reported to be about 40–100 Hz [19]. Fast STOs in spinal motoneurons can be generated from the interplay between the fast, transient sodium current and two potassium currents: the delayed-rectifier current and an afterhyperpolarization (AHP) current. The time scale of the first two currents and the third current were reported to be 1 and 10 ms, respectively. MMOs were found to emerge from the Shilnikov bifurcation of the resting state [19].

The current study deals with four unanswered questions: Which mechanisms can lead to MMOs generation in vibrissa motoneu-

rons? How can they be distinguished based on the properties of their firing patterns? Is the mechanism in vibrissa motoneurons different from that of spinal motoneurons [19]? What are the functional advantages for motoneurons to be in the MMO mode? This is done by analyzing a conductance-based model in vibrissa motoneurons that can exhibit MMO activity [15].

Results

Model of a vibrissa motoneuron

The single compartment, conductance-based model for a vibrissa motoneuron was described in [15]. In brief, the current balance equation is

$$C\frac{dV}{dt} = -g_L(V - V_L) - I_{Na} - I_{NaP} - I_{Kdr}$$
$$- I_{AHP} - I_M - I_h + I_{noise} + I_{app} \qquad (1)$$

where V is the membrane potential of the neuron, $C = 1\ \mu F/cm^2$ is the membrane capacitance of the neuron, and the parameters of the leak current are $g_L = 0.12\ mS/cm^2$ and $V_L = -70\ mV$ (see "Ionic currents of the model" in Methods). The applied current injected into the neuron is denoted by I_{app}, which is considered to be constant in time unless otherwise stated. The ionic currents consist of the transient Na^+ current, I_{Na}; the persistent Na^+ current, I_{NaP}; the delayed rectifier K^+ current, I_{Kdr}; the slow AHP, Ca^{2+}-dependent K^+ current, I_{AHP}; the slow voltage dependent, K^+ current, I_M; and the hyperpolarization-activated h-current I_h. The noise current is $I_{noise}(t) = \sigma \xi(t)$ [20], where $\xi(t)$ is a Gaussian white noise: $<\xi(t)> = 0$ and $<\xi(t)\xi(t')> = \delta(t-t')$; $<...>$ means average over trials and δ is the Dirac function (see [21]). The units of σ are $\mu A \times ms^{1/2}/cm^2$. The value of $\sigma = 0$ is used unless stated otherwise.

STOs in noiseless neurons with $g_h = 0$

The first step is to investigate the neuronal dynamics with no h-conductance. This case is studied for two reasons. First, it is simpler than the case with $g_h > 0$. Second, the dynamical regimes defined for $g_h = 0$ provide the basis over which more complicated dynamics for $g_h > 0$ are identified. The relationship between the firing pattern and I_{app} in the model depends on the M-type K^+ conductance, g_M. For small g_M, there is a transition from a rest state to a firing state as I_{app} increases. For example, the bifurcation diagram for $g_M = 0.4\ mS/cm^2$ (Figure 1A) shows that the rest state is destabilized via a subcritical Hopf bifurcation, and a firing state with a frequency of a few Hz emerges. There is a narrow bistable regime [22]. At intermediate g_M values, such as $g_M = 1\ mS/cm^2$ (Figure 1B), the rest state is destabilized via a supercritical Hopf bifurcation, and a state of STOs emerges. This state switches abruptly to a firing state at a large I_{app} value. This abrupt switch corresponds to the canard scenario [23]. Examples of convergence to these three states – rest, STO and firing – in response to step currents are shown in Figures 1B₁₋₃. When g_M further increases, the resting state is destabilized again by a subcritical Hopf bifurcation, this time with an extended bistable regime (Figure 1C), and there are no STOs.

The phase diagram in the I_{app}–g_M plane shows that STOs are obtained in a restricted I_{app} regime, between a regime of quiescence and a regime of tonic firing. For STOs to occur, g_M should be neither too small nor too large ($0.42\ mS/cm^2 < g_M < 1.33\ mS/cm^2$; Figure 2A). The I_{app} value for which STOs emerge increases with g_M. The I_{app} range in which STOs occur increases and then decreases with g_M. For STOs to occur, the persistent

sodium conductance g_{NaP} should also be within intermediate values ($0.035\ mS/cm^2 < g_{NaP} < 0.057\ mS/cm^2$; $g_M = 1\ mS/cm^2$; Figure 2B). The I_{app} value for which STOs emerge decreases with g_{NaP}. The I_{app} range in which STOs occur increases and then decreases with g_{NaP}. No MMOs were observed in the noiseless model without g_h.

MMOs in noiseless neurons with g_h

When the h conductance g_h is larger than zero, bifurcation diagrams of the model neurons (Figure 3A) resemble those for the case where $g_h = 0$ (Figure 1B). For the reference parameter set ($g_M = 1\ mS/cm^2$), the system switches from a rest state (Figure 4A) to STOs (Figure 4B) as I_{app} increases. These STOs are destabilized via a period doubling (PD) bifurcation at $I_{app} = I_{PD}$. At $I_{app} = I_{SNP}$ ($I_{SNP} > I_{PD}$) there is a saddle-node of periodics (SNP) bifurcation. The neuron fires tonically for $I_{app} > I_{SNP}$ (Figure 4H). There is, however, one major difference between the model with and without g_h. For $g_h > 0$, there is a range of I_{app} between I_{PD} and I_{SNP} where no simple attractor (rest state or tonic firing) exists. Instead, the model neuron exhibits MMOs characterized by subthreshold oscillations between spikes (Figures 3, 4C–G).

The number of STOs between two consecutive spikes decreases with I_{app}, whereas the STO frequency depends only weakly on I_{app} (Figure 4). As a result, the average firing rate during the MMO state increases with I_{app} (Figure 3B). In most cases (e.g., Figure 4C–E,G), but not all (e.g., Figure 4F) the MMO state is periodic. The labeling method of [23] is thus modified to define the state during periodic MMOs by indicating the number of spikes (as regular numbers) and STOs (as superscripts) in consecutive episodes within one time period. The states shown in Figure 4B–H are therefore: B. 0^1 is (an STO state). C. 1^3. D. $1^1 1^2$. E. 1^1. F. Aperiodic state. G. 2^1. H. 1^0 (tonic firing). The 1^1 state occupies the largest I_{app} range (Figure 3B). For smaller values of I_{app}, the firing pattern resembles 1^n for most of the I_{app} interval, where n is an integer. For the reference parameter set, the maximal n is 5. There are narrower ranges where the firing patterns are more complicated, such as $1^1 1^2$. Aperiodic, probably chaotic patterns are also found. For I_{app} values larger than that of the 1^1 range, the neuron fires mostly in n^1 patterns, and n increases with I_{app}. For large enough I_{app} the firing patterns switch to 1^0 and the neuron fires tonically without STOs between spikes. The graph of the firing rate f_R as a function of I_{app} (Figure 3B) has a Devil's staircase shape [24].

The phase diagram in the I_{app}–g_h plane (Figure 5) shows that MMOs are obtained between an STO regime and a tonic firing regime. The I_{app} range in which MMOs are obtained increases approximately linearly with g_h; it approaches 0 as $g_h \to 0$. The I_{app} range in which the neuron exhibits STOs varies only weakly with g_h.

Noise-induced MMOs

Individual ionic channels are discrete elements whose properties can be given only probabilistically [25]. Spontaneous synaptic release is also probabilistic [26]. In neuronal modeling, this stochastic dynamics are often modeled by adding white stochastic, Gaussian noise to the underlying deterministic dynamics [20]. Here, a second mechanism for MMOs generation is considered, in which stochastic noise leads to MMOs firing patterns when the noiseless neuron exhibits STOs or even quiescence or tonic firing. To analyze noise effects, the properties of the motoneuron model with a nonzero noise amplitude σ were studied. To show the impact of parameter σ, the model was simulated in a regime where it is at rest for $\sigma = 0$ (no spikes, STOs or MMOs). Here, weak or moderate noise generates voltage fluctuation but not
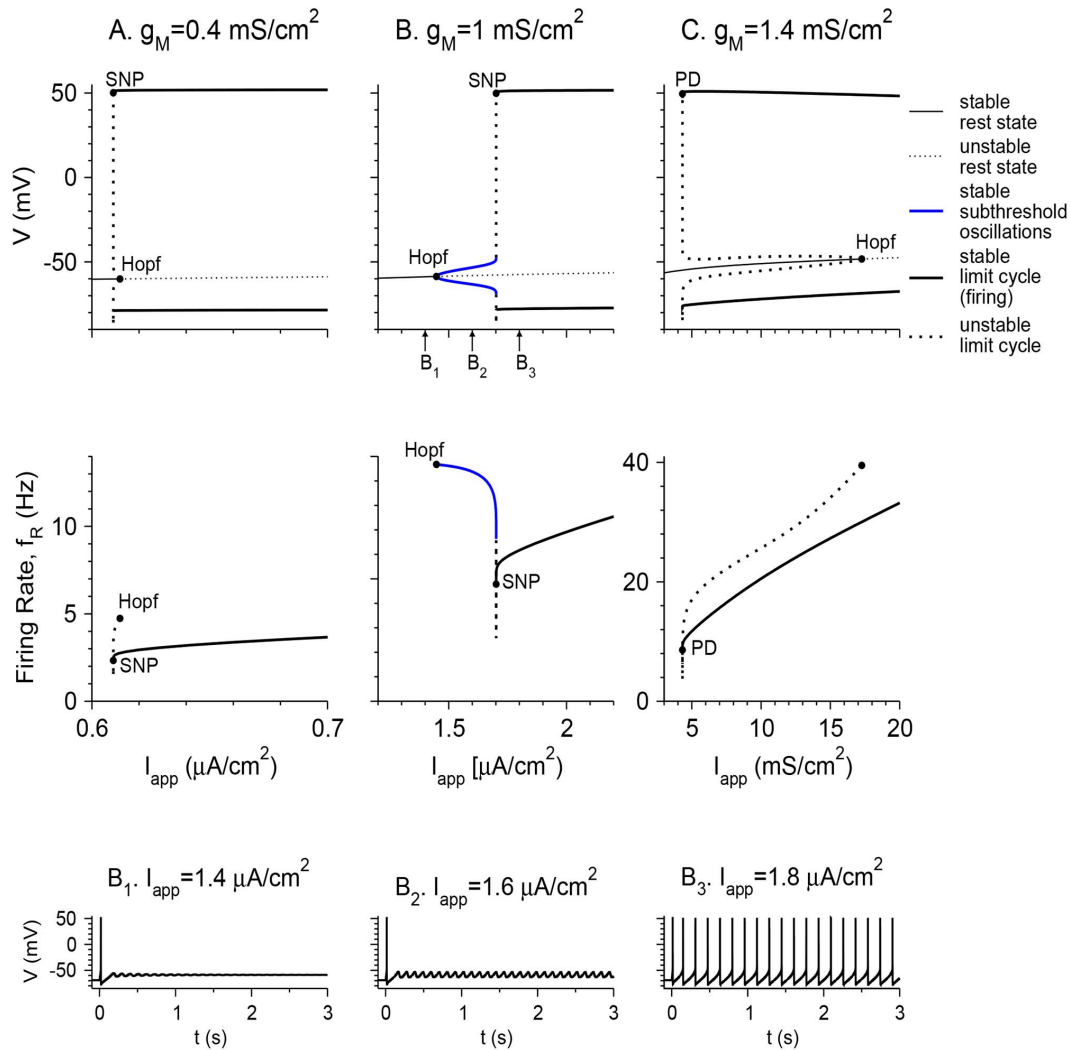
Figure 1. Bifurcation diagrams of the vibrissa motoneuron model with $g_h = 0$. The values of the membrane potential V (top panels) and the firing rate f_R (medium panels) are plotted as functions of I_{app} for fixed points (thin lines) and limit cycles (thick lines) for $g_M = 0.4$ mS/cm^2 (A), $g_M = 1$ mS/cm^2 (B) and $g_M = 1.4$ mS/cm^2 (C). For limit cycles, minimal and maximal voltages during the cycle are plotted. Solid lines denote stable solutions, and dotted lines denote unstable solutions. Stable sub-threshold oscillations are shown in blue, whereas stable tonic firing states are shown in solid thick black lines. Solid circles denote bifurcations from the following types: Hopf (HB), saddle-node of periodics (SNP) and period doubling (PD). Panels B_1-B_3 at the bottom present the voltage time traces for $g_M = 1$ mS/cm^2 and $I_{app} = 1.4$, 1.6 and 1.8 μA/cm^2 respectively. These I_{app} values are denoted by the arrows below the abscissa in panel B (top).
doi:10.1371/journal.pone.0109205.g001

spikes (Figure 6A). The standard deviation of the fluctuations σ_V is defined as

$$\sigma_V = \left[\langle V^2(t) \rangle_t - \langle V(t) \rangle_t^2 \right]^{1/2} \qquad (2)$$

where $\langle ... \rangle_t = (1/T) \int_0^T dt...$ means time average over a large time T. The standard deviation σ_V increases linearly with σ for small σ (Figure 6B), and spikes are observed for large enough σ. Spikes are not observed for σ values below 0.1 μA$\times$ms$^{1/2}$/cm^2, that yield voltage fluctuations below 2 mV.

Noise may generate MMOs when they do not exist for the noiseless neuron, or increase their range of appearance when they do. First, I study a case in which the noiseless neuron does not exhibit MMOs: $g_h = 0$, $g_M = 1$ mS/cm^2. It exhibits STOs for I_{app} between $I_{HB} = 1.45$ μA/cm^2 and $I_{PD} = 1.7$ μA/cm^2 (Fig. 1B). It spikes tonically for $I_{app} > I_{PD}$. A (relatively small) noise level of

$\sigma = 0.01$ μA$\times$ms$^{1/2}$/cm^2 transfers STOs or tonic spiking activity to MMOs in the I_{app} in a restricted range around I_{PD} (Figure 7A$_{2,3}$), but not far from that value (Figure 7A$_{1,4}$). Increasing σ expands the range of noise-generated MMOs ($\sigma = 0.1$ μA$\times$ms$^{1/2}$/cm^2; Figure 7B). Second, I study a case in which the noiseless neuron can exhibit MMOs: $g_h = 0.3$ mS/cm^2, $g_M = 1$ mS/cm^2 (Figure 5). Small levels of noise such as $\sigma = 0.01$ μA$\times$ms$^{1/2}$/cm^2 only enlarge the MMO regime mildly (Figure 7C). Large noise levels also cause the generation of MMO patterns in the regime where, without noise, the neuron exhibits STOs or fires tonically ($\sigma = 0.1$ μA$\times$ms$^{1/2}$/cm^2; Figure 7D) or even when is silent ($\sigma = 0.32$ μA$\times$ms$^{1/2}$/cm^2; not shown).

Effects of noise on the appearance of MMOs are also demonstrated by plotting the firing rate and the coefficient of variation (CV) of the model neuron as a function of I_{app} when there are no MMOs without noise ($g_h = 0$; Figure 8A$_{I,II}$) and when the noiseless neuron can exhibit MMOs ($g_h = 0.3$ mS/cm^2; Figure
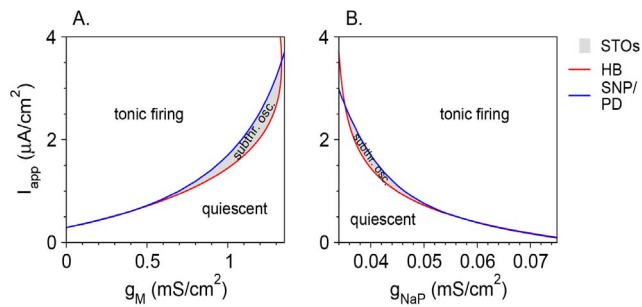
Figure 2. Phase diagrams of the vibrissa motoneuron model with $g_h = 0$. The dynamical states of the model neuron are plotted in the g_M-I_{app} plane (A) and in the g_M-I_{app} plane (B). A regime of STOs (light grey) is obtained between the regimes of quiescence and tonic firing. Red lines denote the Hopf bifurcation (HB), and blue lines denote the saddle-node of periodics (SNP) or period doubling (PD) bifurcations.
doi:10.1371/journal.pone.0109205.g002

8B$_{I,II}$). In the first case, the regime of noise-induced MMOs is characterized by firing rates between that of tonic firing (around 6 Hz here) and 0, and by CV values between 0 and 1. For all levels of noise, the firing rate increases with I_{app} and CV decreases with it, since temporal maxima in $V(t)$ correspond more frequently to spikes than to sub-threshold oscillations. A different situation is found when MMOs are observed without noise ($g_h = 0.3$ mS/cm^2). For $\sigma = 0$, the firing rate as a function of I_{app} exhibits a Devil's staircase shape, and the CV fluctuates between 0 and positive values that have maxima around 0.08–0.28. This occurs because CV is 0 when the number of STOs between each pair of consecutive spikes is fixed; namely the state is 1^n for any n (with fixed n for all t; Figure 4C,E). As I_{app} increases, the neuron tends to fire in more complex periodic manner (Figure 4D), aperiodically (Figure 4F), or in modes such as n^1 (figure 4G). In all such firing patterns, CV is positive. It goes back to 0 when the neuron switches to tonic firing (Figure 4H). Adding a small amount of noise smooths the firing rate versus I_{app} curve as well as the CV curve, and extends the I_{app} interval in which MMOs are observed on both sides. The CV is large (~ 0.7–1) when MMOs begin to emerge as I_{app} increases, but then decreases as the firing patterns become similar to the MMOs observed for $\sigma = 0$. As I_{app} increases further, the CV increases as it follows a smooth version of the curve for $\sigma = 0$, and then decreases again to near zero as the firing pattern switches to tonic firing. The CV vs. I_{app} (or vs. f_R) curve is therefore non-monotonous and has an N-shape form for moderate levels of noise. Only for large noise levels ($\sigma = 0.1$ μA×ms$^{1/2}$/cm^2 and above in Figure 8) does the CV decrease monotonically with I_{app} whereas the firing rate increases monotonically with it.

To further explore non-random firing patterns in the case where MMOs are generated by the effect of both an intrinsic mechanism and noise, the firing rate f_R and the coefficient of variation CV are computed in a simple model. In this simple model, the membrane potential V of a neuron oscillates between a high and a low voltage with a time period t_p. When V reaches its maximal value, the neuron either fires a spike at random with a probability p or does not fire and goes back to its minimal value with a probability of 1-p. The spike duration is very small and refractoriness is neglected, such that the time period between two consecutive maxima of V does not depend on whether the peak occurs during a spike or a maximum V value of an STO, under a Bernoulli process [27]. The average inter-spike interval ($<$ISI$> = 1/f_R$) is geometrically distributed (see "a simple model of MMOs generated by noise alone" in Methods) with an average t_p/p, variance $t_p^2(1-p)/p^2$ and CV $\sqrt{1-p}$. Therefore, for a Bernoulli process,
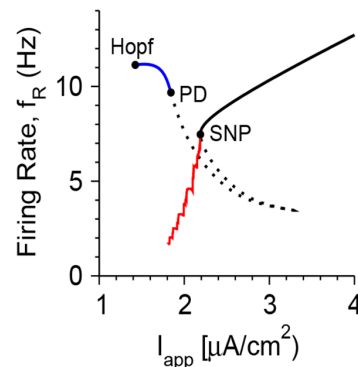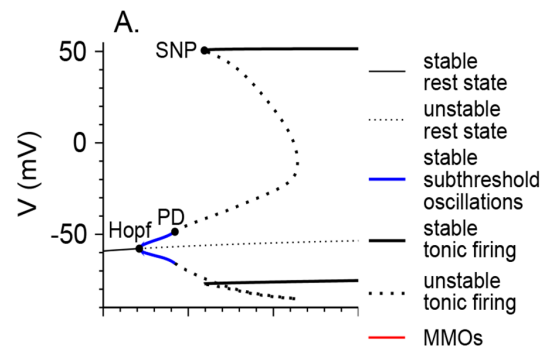

Figure 3. Bifurcation diagrams of the vibrissa motoneuron model with $g_h = 0.3$ mS/cm^2. (A) The values of the membrane potential V (top panel) and the firing rate f_R (bottom panel) are plotted as functions of I_{app} for fixed points (thin lines) and limit cycles (thick lines) for $g_M = 1$ mS/cm^2. For limit cycles, minimal and maximal voltages during the cycle are plotted. Solid lines denote stable solutions, and dotted lines denote unstable solutions. Stable sub-threshold oscillations are shown in blue, whereas stable tonic firing states are shown in solid thick black lines. Solid circles in the top panels denote bifurcations from the following types: Hopf (HB), saddle-node of periodics (SNP) and period doubling (PD). The firing rate in the MMOs state is plotted in red in the bottom panel. (B) The firing rate f_R in the MMOs state is plotted as a function of I_{app} at a larger scale. The types of mixed mode states (see text, Figure 4 and [23]) are indicated above the curve.
doi:10.1371/journal.pone.0109205.g003

$$t_p = f_R(1 - CV^2) \qquad (3)$$

Since the STO frequency that underlies MMOs depends only weakly on I_{app}, if the spiking can in fact be well described by a Bernoulli process, then predicting t_p from f_R and CV should display a weak dependence on I_{app}. In fact, for large σ

Figure 5. Phase diagram of the vibrissa motoneuron model in the g_h-I_{app} plane. Regimes of STOs (light grey) and MMOs (dark grey) are obtained between the regimes of quiescence and tonic firing. The red line denotes Hopf bifurcation (HB), the green line denotes period doubling (PD) bifurcation, and the blue line denotes saddle-node of periodics (SNP) bifurcation.
doi:10.1371/journal.pone.0109205.g005

calculated values of t_p in the regime where the noiseless neurons exhibits STOs are below what is expected from Eq. 3. This is because CV is close to 1, beyond what is expected from a Bernoulli process. The model neuron tends to fire in clusters of spikes (Figure 7B$_1$). An explanation of this behavior is beyond the scope of this article.

Response of a motoneuron pool to constant and periodic inputs

There are about 50–100 motoneurons projecting to each vibrissa muscle [1,4], with no chemical or electrical synapses among them. These neurons receive periodic stimulation from the vIRT or the Bötzinger nuclei [10], and are also slowly modulated

Figure 6. Voltage fluctuations generated by stochastic noise. (A) Voltage time traces of the model neurons with $g_M = 1$ mS/cm^2, $g_{NaP} = 0.04$ mS/cm^2, $g_h = 0$, $I_{app} = 1.4$ μA/cm^2, $\sigma = 0.032$ μA×ms$^{1/2}$/cm^2. For $\sigma = 0$, the model neurons are at rest for this parameter set. With noise, the membrane potential fluctuates. (B) The standard deviation of the voltage σ_V as a function of the noise level σ. This figure demonstrates how the noise strength affects the magnitude of voltage fluctuations without any intrinsic STOs mechanism.
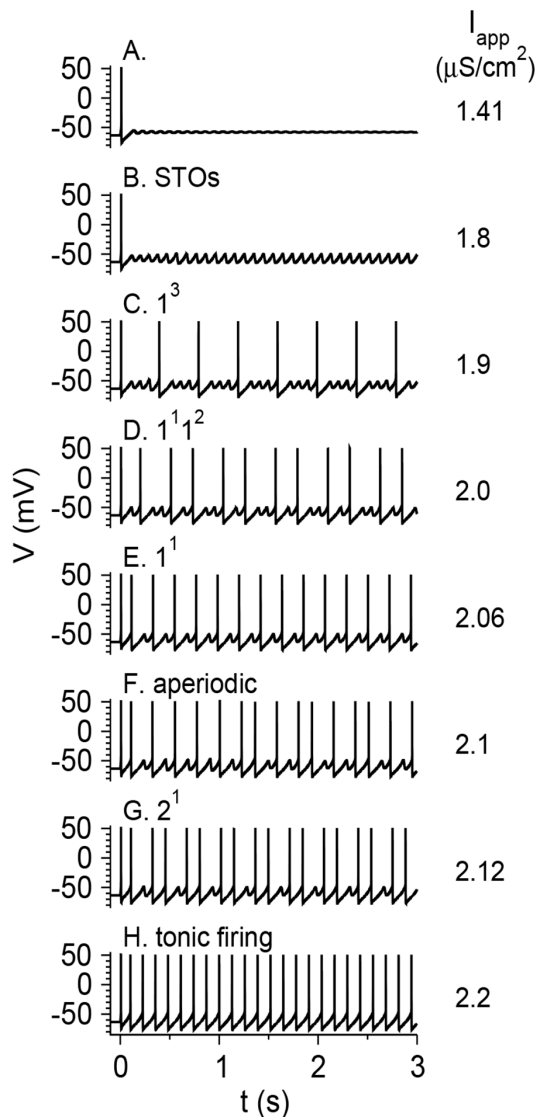doi:10.1371/journal.pone.0109205.g006

Figure 4. Voltage time traces of the model neuron in response to step current injection at $t=0$. Parameters are as in Figure 3 ($g_h = 0.3$ mS/cm^2). The values of I_{app} are written in units of μA/cm^2. (A) $I_{app} = 1.41$, the membrane potential of the neuro goes to rest. (B) $I_{app} = 1.8$, the neuron exhibits sub-threshold oscillations. (C) $I_{app} = 1.9$, the neuron fires in an MMOs mode, with 3 sub-threshold oscillations between each pair of consecutive spikes. (D) $I_{app} = 2.0$, the neuron fires in an MMOs mode. The number of STOs between pairs of consecutive spikes switches alternately between 1 and 2. (E) $I_{app} = 2.06$, the neuron fires in an MMOs mode with one STO between two consecutive spikes. (F) $I_{app} = 2.1$, the neuron fires aperiodically. (G) $I_{app} = 2.12$, The neuron fires two spikes, shows one STO, and then the cycle starts again. (H) $I_{app} = 2.2$, the neuron fires tonically. The dynamical states are indicated above each panel.
doi:10.1371/journal.pone.0109205.g004

(0.32 μA×ms$^{1/2}$/cm^2), t_p weakly decreases with I_{app}, as takes place for tonic spiking with no noise (Figure 8A$_{III}$ and 8B$_{III}$, orange). In contrast, for small and moderate noise levels, t_p strongly increases as I_{app} decreases, by about a factor of 5, within the I_{app} regime where without noise, the model neurons exhibit MMOs (and even when they exhibit STOs). This behavior is caused by the low values of CV with respect to what is expected from a Bernoulli process, which stem from the fact that the MMOs are generated by an intrinsic neuronal mechanism. Note that for $g_h = 0$, the
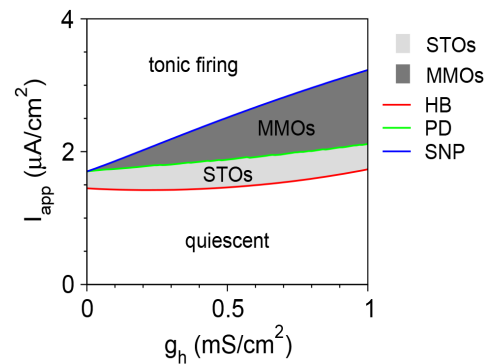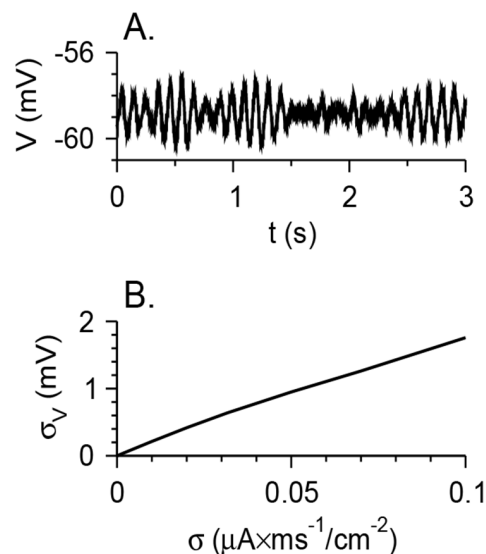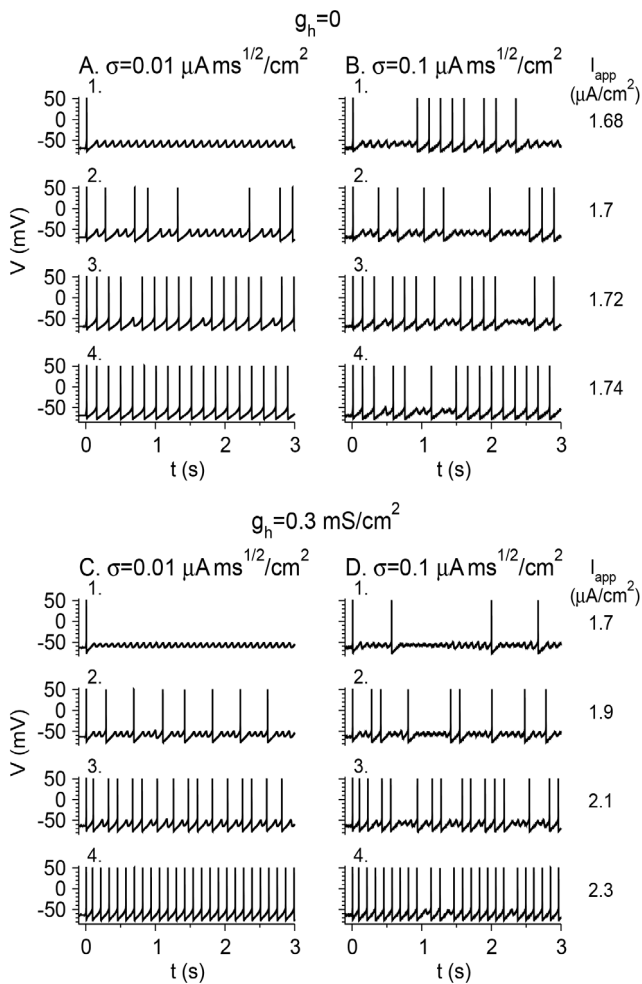
Figure 7. Voltage time traces of the model neuron in response to step current injection at $t=0$. The values of I_{app} are indicated to the right of the traces. (A) $g_h = 0$, $\sigma = 0.01$ μA×ms$^{1/2}$/cm^2. The noiseless neuron does not exhibit MMOs, but this level of noise generates MMOs near the transition between quiescence and tonic firing. (B) $g_h = 0$, $\sigma = 0.1$ μA×ms$^{1/2}$/cm^2. For this larger noise level, MMOs are generated in a more widespread I_{app} regime. (C) $g_h = 0.3$ mS/cm^2, $\sigma = 0.01$ μA×ms$^{1/2}$/cm^2. The noiseless neuron generates MMOs. This level of noise increases the I_{app} regime in which MMOs are obtained only slightly. The MMOs are less ordered, and the number of STOs between spikes varies from one inter-spike interval to another. (D) $g_h = 0.3$ mS/cm^2, $\sigma = 0.1$ μA×ms$^{1/2}$/cm^2. MMOs appear in I_{app} regimes in which the noiseless neuron is quiescent or fires tonically, and the firing patterns look less ordered.
doi:10.1371/journal.pone.0109205.g007

by serotonin that increases their excitability [12]. To assess the ways in which the two stimuli control the activity of a motoneuron pool controlling cells in a single muscle, a simulation is tested on a pool of $N = 50$ uncoupled motoneurons (N is the number of neurons) with $g_h = 0.3$ mS/cm^2 and a noise level $\sigma = 0.032$ μA×ms$^{1/2}$/cm^2, that differ only by the realization of the noise (i.e., with different seeds for the noise of different neurons [28]). The excitability of the neurons, controlled naturally by neuromodulations and quantified here by I_{app}, is within or around the MMOs regime. All the neurons are stimulated by the same periodic input, which is I_c during the first 20 ms of the period $T_{per} = 1/f$ and 0 otherwise (Figure 9). For moderate values of I_c and values of f around the frequency of peaks (of STOs or spikes) of the non-stimulated neurons, the MMO nature of the dynamics

is maintained, and the stimulus simply locks the spikes to its pace (Figure 9A). Since the firing frequency is lower than the peak frequency, different neurons with different noise realizations will not necessarily fire during the same stimulus period. If, on average, the neuron fires every n cycles of the stimulus, the number of spikes in each stimulus will be on average N/n, as shown in the rastergram in Figure 9B for $I_{app} = 2$ μA/cm^2 and $I_c = 0.15$ μA/cm^2. While most neurons fire during the "up" phase of the stimulus, some neurons fire somewhat later. To quantify the level of synchrony of the motoneuron pool, the total force developed in the muscle is computed. It is assumed that each spike, fired at time t_s, generates a force twitch in the cells it innervates

$$f(t) = \frac{A}{\tau_2 - \tau_1}\left(e^{-(t-t_s)/\tau_2} - e^{(-t-t_s)/\tau_1}\right)\Theta(t-t_s) \qquad (4)$$

where Θ is the Heaviside function, $\tau_1 = 5$ ms and $\tau_2 = 6$ ms [29] and $A = 1$ in arbitrary units. The force contributions of motor units (i.e., muscle cells that are innervated by the same motoneuron) are summed linearly. The total muscle force F, plotted in Figure 9C, shows that the motoneuron spikes are partially synchronized [30]. The amplitude, however, is about twice as small as the force amplitude developed for $I_{app} = 2.4$ μA/cm^2, for which the isolated neuron fires every cycle (Figure 8C). These results reflect the following motor control scenario: when the non-stimulated motoneurons are in or around the MMOs regime, and motoneurons function under the effects of neuromodulators such as serotonin, the firing frequency is controlled by a moderate periodic frequency whereas the firing amplitude can be controlled by neuromodulators.

Discussion

Summary of the results

Experimentally, vibrissa facial motoneurons may fire in a mixed mode oscillation (MMO) state in response to constant current injection I_{app} [12,14]. This firing mode affects the integration of synaptic and neuromodulatory inputs. This study investigated the generation of MMOs using a computational model [15]. A noiseless model does not exhibit MMOs without h conductances, but subthreshold oscillations (STOs) are obtained with moderate values of g_M and g_{NaP} (Figures 1,2). Addition of the h-type conductance g_h enables the generation of MMOs, with a firing frequency that depends on I_{app} like a Devi's staircase (Figures 3,4). The MMO range increases linearly with g_h (Figure 5). Small levels of stochastic noise increase the MMO regime by converting STOs or tonic firing to MMOs, often with CV values significantly lower than 1. Large noise levels generate MMOs with firing statistics indicating a Bernoulli process. Based on these results, it is possible to determine which one of three MMO mechanisms generates MMOs in a neuron based on intracellular recordings. This study shows how, by using the MMO mode, fast synaptic and slow neuromodulatory inputs can control the frequency and amplitude of whisking, respectively.

Comparison of spinal and vibrissa motoneuron firing patterns

Mixed mode oscillations are found experimentally in both rat [18] and mouse [19] spinal motoneurons, as well as rat vibrissa motoneurons. In these cases, conductance-based models reveal MMOs as well. In experiments and models of the two types of motoneurons, persistent inward conductances such as g_{NaP} are needed to obtain MMOs [18]. In models of both types, adding noise extends the MMO range and makes the discharge more
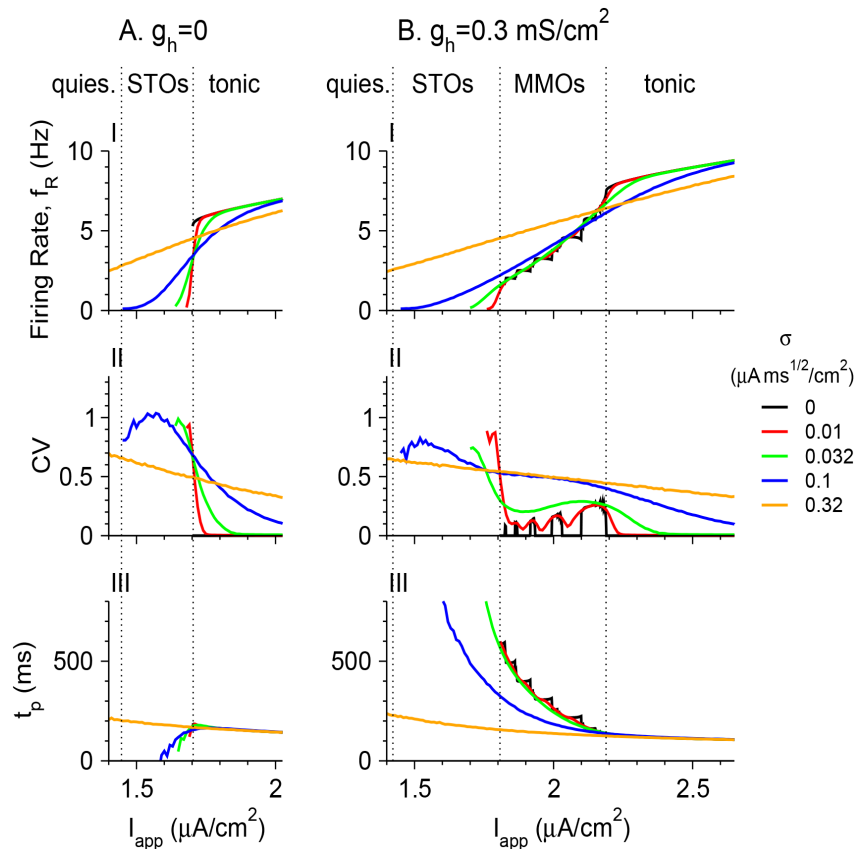
Figure 8. Properties of firing patterns without and with an intrinsic MMOs-generating mechanism. The firing rate f_R (I), the coefficient of variation CV (II) and the time period t_p, computed assuming a Bernoulli process (Equation 3) (III) are plotted as a function of I_{app} for $g_h = 0$ (A) and $g_h = 0.3$ mS/cm^2 (B). The colors of the lines denoting the values of σ (in $\mu A \times ms^{1/2}/cm^2$) are: black – 0, red – 0.01, green – 0.032, blue – 0.1 and orange – 0.32. The vertical dotted lines denote the I_{app} values of the transitions between different dynamical states (quiescence, STOs, MMOs and tonic firing) of the noiseless neuron.
doi:10.1371/journal.pone.0109205.g008

irregular. There are, however, major differences between the firing patterns of these two types of motoneurons. The firing rate of rat vibrissa motoneurons, as well as the MMO frequency, is about 5–10 Hz [7,14], which is substantially lower than that of spinal motoneurons of rats [18] and mice [19], which is about 20–100 Hz. Therefore, the h-conductance with kinetics on the order of 100 ms, which is critical for generating MMOs in the model presented here, is not expected to play a major role in spinal motoneurons dynamics. In fact, it is sufficient to generate MMOs in a "minimal" model of spinal motoneurons with only transient Na$^+$, delayed rectifier K$^+$ and M-like K$^+$ conductances [19], whereas in the present model additional g_{NaP} and g_h are needed. Another important difference has to do with the behavior just outside the I_{app} regime where MMOs emerge. In the present model the neuron exhibits STOs at I_{app} values just below those where MMOs exist. This behavior occurs because as I_{app} is increased, the rest state is first destabilized by a *supercritical* Hopf bifurcation (HB) (Figure 5), and MMOs are only observed after a period doubling (PD) bifurcation at a further larger I_{app} value. In contrast, in the spinal motoneuron model there is no STO regime, since the rest state is destabilized by a *subcritical* HB while a homoclinic trajectory arises (Shilnikov's homoclinic bifurcation scenario; see Figure 8 in [19]). Therefore, the existence of an STO regime points to which mechanism is responsible for intrinsic MMOs generation.

In the Shilnikov scenario, the dynamical system escapes spirally from an unstable fixed point [31]. This implies that for spinal motoneurons, the MMO amplitude increases from cycle to cycle until the neuron fires a spike, as shown both experimentally and in the model [19]. In contrast, in the present model the amplitudes of membrane potential oscillations remain constant between spikes (Figures 4,7). The method suggested here serves to determine whether MMOs are generated by the intrinsic mechanism based on g_h described in this work, or by that of [19]. Specifically, the intrinsic mechanism analyzed here exhibits a significant regime of STOs in I_{app} values below the MMOs regime, and the STOs amplitude is about constant with time. In the Shilnikov-based spinal motoneuron mechanism, there are no STOs for lower I_{app} values, and the STO amplitude increases with time. These different firing types can be distinguished based on intracellular recording.

Distinguishing an intrinsic from a noise-induced mechanism

MMOs can be generated by an intrinsic mechanism, or by stochastic noise that transforms an STO state, a quiescent state, or a tonic firing state into an MMO state. The method presented here distinguishes between these two options based on recordings of the firing patterns for varying values of I_{app}. The first step is to measure or compute the firing rate f_R and the coefficient of variation CV as functions of I_{app}. An increase in f_R, together with
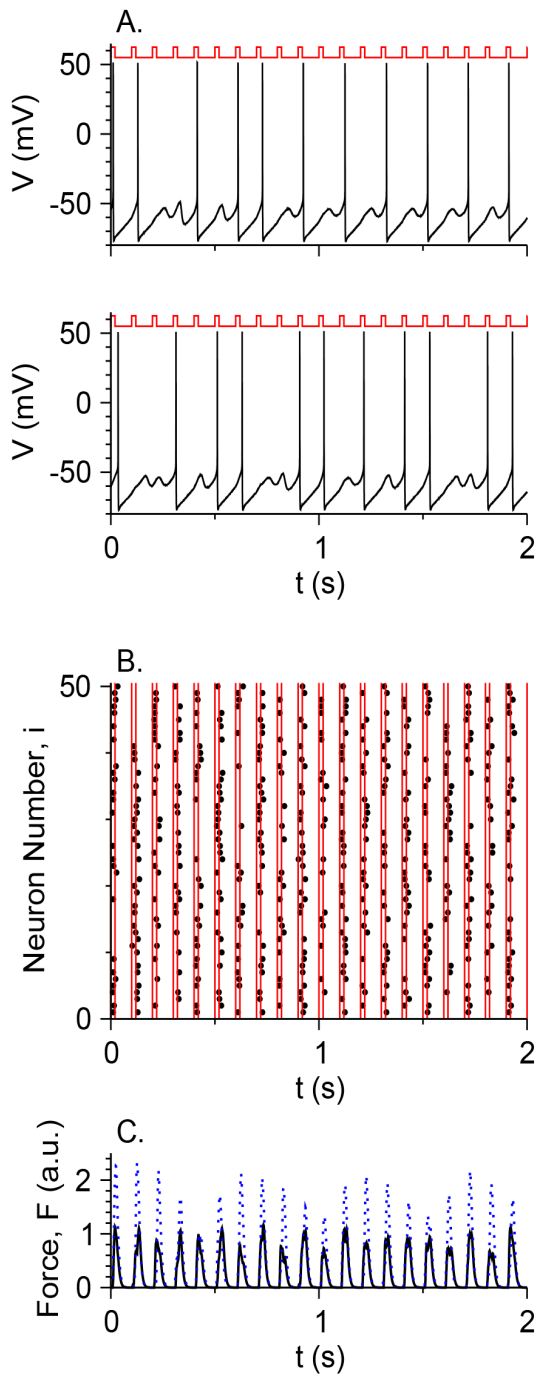
Figure 9. Response of a motoneuron pool to periodic stimulation from a CPG and neuromodulation. 50 uncoupled motoneurons are simulated, each receiving constant input $I_{app} = 2$ μA/cm^2 mimicking the excitability effects of neuromodulators such as serotonin, and periodic stimulation from a CPG with a frequency $f = 10$ Hz. The periodic stimulation is $I_c = 0.15$ μA/cm^2 during the first 20 ms of each cycle with a duration of $T_{per} = 1/f$, and 0 otherwise. Different neurons have different noise realizations. Additional parameters: $g_h = 0.3$ mS/cm^2, $\sigma = 0.032$ μA×ms$^{1/2}$/cm^2. Realizations of the noise are different across motoneurons. (A) The membrane potential V as a function of t for two neurons (black). The stimulus pattern is schematically plotted above each panel (red) to emphasize the synchrony of spikes with the stimulus. (B) Rastergram of the spikes (black circles) of the 50 motoneurons. The stimulus is I_c between each pair of adjacent red lines. (C) The total force amplitude F, in arbitrary units ($A = 1$, Equation 4), generated by a whole muscle whose cells are innervated by the pool of motoneurons (black). The dotted blue line denotes a similar simulation with $I_{app} = 2.4$ μA/cm^2.
doi:10.1371/journal.pone.0109205.g009

a smooth decrease of CV as a function of I_{app} indicates that the STOs are generated by noise, although this cannot rule out the existence of an intrinsic mechanism for MMOs that is smeared out by large noise (Figure 8). If f_R increases with I_{app} and CV varies non-monotonically with I_{app}, there is an intrinsic mechanism underlying the MMO firing pattern. Another method is to compute the time period t_p between peaks of oscillations (either STOs or spikes) assuming a Bernoulli process according to Equation 3. If there is a range of I_{app} where f_R rises by an order of magnitude while t_p decreases by the same order, this is an indication of an intrinsic mechanism.

MMOs in various types of neurons and models

In the present model with $g_h = 0$, the transition between STOs and tonic firing is abrupt, reminiscent of a canard transition [32,33] (Figure 1B). For $g_h > 0$, the STOs are destabilized via a PD bifurcation, MMOs are generated, and tonic firing is restored via an SNP bifurcation (Figure 3). A similar bifurcation scenario was observed in a model of fast-spiking cortical neurons [23]. That model did not include h-conductance, but rather implemented a K$^+$ conductance g_{Ks} that was slow at hyperpolarized potential. MMOs were observed only if g_{Ks} was above a certain positive critical value. In contrast, in the present model, MMOs are observed in vibrissa motoneurons for any positive value of g_h. The reason for this effect is unknown.

In addition to motoneurons, MMOs have been observed in other neuronal types. For example, MMOs with frequencies of a few Hz were observed in cortical interneurons [34], pyramidal cells of the frontal cortex [35], and stellate cells of the entorhinal cortex [36–38]. The conductances g_{NaP}, g_M and g_h were found to be important for the generation of MMOs in the enthorhinal cortex [39,40], and stochastic noise contributes to them as well [41,42]. In another model of these neurons [43], STOs (but not MMOs) emerged from the interplay between I_{NaP} and I_h. In the present model neither subthreshold oscillations nor mixed-mode oscillations are observed without I_M. This difference between the present model and the one described in [43] stems from the fact that θ_r, the half-maximum potential of the activation curve of I_h in the present model (see "Ionic currents of the model" in Methods) is about 14–17 mV more hyperpolarized than the resting potential, whereas θ_r in the Dickson et al. model [43] is more *depolarized* than at rest by 11–21 mV; hence the h current is more effective at membrane potentials near spike threshold. In the present model, the value for θ_r is consistent with the experimental observation by Hattox et al. [12] in vibrissa motoneurons, showing that the sag effect is substantial only much below resting potential. Mixed mode oscillations have been found in models of layer 5 pyramidal neurons [44] and in the Hodgkin-Huxley model of the squid giant axon when the activation time constants τ_h or τ_n were reduced, as a result of the "canard" effect [45].

Functional significance

Control the whisking frequency and whisking amplitude in a coordinated manner, both between motoneurons that project to the same muscle and those that project to different muscles, is a challenge to the nervous system [46]. Since vibrissa facial motoneurons are uncoupled [8], and about 50–100 motoneurons project to each muscle, this coordination needs to emerge from the inputs to the motoneurons. The most obvious sources are the rhythmic input from the vIRt and Bötzinger nuclei in the

brainstem [10,11] and serotonergic modulation [12], although sensory feedback from the trigeminal ganglion [16] may affect motoneuron firing. If neurons are "standard" class I or II types [22,47], neuromodulation can abruptly transform them from a silent state to a tonically active state, but the interaction of the rhythmic input with the tonically-firing neurons may generate complex firing patters. In their work on spinal motoneurons, Iglesias et al. [19] suggested that MMO patterns can be used to make the transition between quiescence and a high firing rate more moderate by reducing the neuronal gain. This effect is seen in the vibrissa motoneurons as well (Figure 8). In the whisker system, however, MMOs can serve another purpose.

Here, a control mechanism is suggested based on motoneurons that fire in an MMO mode (Figure 9). Moderate levels of periodic input control the population firing frequency. The serotonergic modulation controls the cell excitability and is modeled here by varying I_{app}. Other possible effects of serotonergic modulation, which are not considered here, may have additional consequences for the network dynamics. The spiking activity of neurons is locked, although not fully, to the "up" state of stimulating periodic activity, whereas the number of STOs between spikes is controlled by the neuromodulation. Increasing the level of cell excitability will increase the number of neurons firing at each period, and, as a result, the whisking amplitude, but the population frequency will remain unchanged. If the intrinsic excitability of the motoneuron population is heterogeneous, the total number of neurons that fire can be controlled in a graded manner. The statistical nature of motor control is consistent with the fluctuations in whisking amplitudes from cycle to cycle [48–50]. In contrast, the fluctuations in the length of consecutive time periods, controlled by the periodic input, can be small, as demonstrated experimentally [4]. This control mechanism enables the division of labor among muscle cells, where each cell contracts once every few cycles [5,51]. In this scenario, intrinsic cellular properties, phasic input and neuromodulation participate in controlling the frequency, phase and amplitude of whisking movement.

Methods

Ionic currents of the model

The following equations and parameters for the ionic currents are implemented [15]. Reference values of parameters are used unless otherwise stated.

Transient Na$^+$ current, I_{Na}: $I_{Na}(V,h) = g_{Na}m_\infty^3(V)h(V - V_{Na})$, $m_\infty(V) = \{1 + \exp[-(V + 28)/7.8]\}^{-1}$, $dh/dt = [h_\infty(V) - h]/\tau_h(V)$, $h_\infty(V) = \{1 + \exp[(V + 50)/7]\}^{-1}$, $\tau_h(V) = 30 \times [\exp((V + 50)/15) + \exp(-(V + 50)/16)]^{-1}$, $g_{Na} = 100$ mS/cm^2, $V_{Na} = 55$ mV.

Persistent Na$^+$ current, I_{NaP}; $I_{NaP}(V,p) = g_{NaP}p_\infty(V)(V - V_{Na})$, $p_\infty(V) = \{1 + \exp[-(V + 53)/5]\}^{-1}$, $g_{NaP} = 0.04$ mS/cm^2.

Delayed rectifier K$^+$ current, I_{Kdr}: $I_{Kdr}(V,n) = g_{Kdr}n^4(V - V_K)$, $dn/dt = [n_\infty(V) - n]/\tau_n(V)$, $n_\infty(V) = \{1 + \exp[(V + 23)/15]\}^{-1}$, $\tau_n(V) = 7 \cdot [\exp((V+40)/40) + (\exp - 1 - (V + 40)/50)]^{-1}$, $g_{Kdr} = 20$ mS/cm^2, $V_K = -80$ mV.

Slow AHP, Ca^{2+}-dependent K$^+$ current, I_{AHP}: based on the work of [52], this activation current is modeled as a voltage-dependent activation with half-maximum potential above threshold. In this form, spikes are needed to activate the AHP channels. $I_{AHP}(V,u) = g_{AHP}u(V - V_K)$, $du/dt = [u_\infty(V) - u]/\tau_u$, $u_\infty(V) = \{1 + \exp[(V + 25)/3]\}^{-1}$, $g_{AHP} = 10$ mS/cm^2, $\tau_u = 75$ ms.

Slow voltage dependent, K$^+$ current, I_M: $I_M(V,z) = g_M z(V - V_K)$, $dz/dt = [z_\infty(V) - z]/\tau_z$, $z_\infty(V) = \{1 + \exp[(V + 45)/4.25]\}^{-1}$, $g_M = 1$ mS/cm^2.

Hyperpolarization-activated h-current I_h: $I_h(V,r) = g_h r(V - V_h)$, $dr/dt = [r_\infty(V) - r]/\tau_r(V)$, $r_\infty(V) = \{1 + \exp[(V + 83.9)/27.4]\}^{-1}$, $\tau_r(V) = 6000 [\exp((V + 140)/21.6) + \exp(-(V + 40)/22.7)]^{-1}$, $V_h = -27.4$ mV g_h is usually set to 0 or 0.3 mS/cm^2.

Numerical methods

Simulations of differential equations without noise were performed using the fourth-order Runge-Kutta method with a time step of 0.01 ms implemented as a C program or within the software package XPPAUT [53]. Simulations of stochastic differential equations were conducted using the Euler method with the same time step. Simulations with a smaller time step (0.001 ms) did not reveal any observable differences. Bifurcation diagrams of deterministic dynamical systems were computed using XPPAUT.

MMOs as a Bernoulli process

The analysis uses a neuron whose voltage oscillates at a time period t_p. Each oscillation peak may become a spike with a probability p or a maximum of an STO with a probability of 1-p. For simplicity, the same t_p is assumed whether the first or second peak of the membrane potential is a spike or an STO. The inter-spike interval (ISI) equals t_p with a probability p and nt_p with a probability of $(1-p)^{n-1}p$ for an integer $n \geq 2$. For this Bernoulli process, the average ISI and ISI^2 are therefore [27]

$$<ISI> = \sum_{n=1}^{\infty} nt_p(1-p)^{n-1}p \qquad (5)$$

$$<ISI^2> = \sum_{n=1}^{\infty} n^2 t_p^2(1-p)^{n-1}p \qquad (6)$$

where $<...>$ represents time-average. I define $q = 1-p$ and use the identities

$$\sum_{n=1}^{\infty} nq^{n-1} = \frac{d}{dq}\sum_{n=1}^{\infty} q^n = \frac{1}{p^2} \qquad (7)$$

$$\sum_{n=1}^{\infty} n(n-1)q^{n-2} = \frac{d^2}{dq^2}\sum_{n=2}^{\infty} q^n = \frac{2(1-p)}{p^3} \qquad (8)$$

to obtain $<ISI> = t_p/p$, $<ISI^2> = t_p^2(2-p)/p^2$, and therefore

$$CV = \frac{(<ISI^2> - <ISI>^2)^{1/2}}{<ISI>} = \sqrt{1-p} \qquad (9)$$

Acknowledgments

Author Contributions

References

1. Herfst LJ, Brecht M (2008) Whisker movements evoked by stimulation of single motor neurons in the facial nucleus of the rat. J Neurophysiol 99: 2821–2832.
2. Dorfl J (1982) The musculature of the mystacial vibrissae of the white mouse. Journal of Anatomy 135: 147–154.
3. Haidarliu S, Simony E, Golomb D, Ahissar E (2010) Muscle architecture in the mystacial pad of the rat. Anat Rec (Hoboken) 293: 1192–1206.
4. Berg RW, Kleinfeld D (2003) Rhythmic whisking by rat: retraction as well as protraction of the vibrissae is under active muscular control. J Neurophysiol 89: 104–117.
5. Hill DN, Bermejo R, Zeigler HP, Kleinfeld D (2008) Biomechanics of the vibrissa motor plant in rat: rhythmic whisking consists of triphasic neuromuscular activity. J Neurosci 28: 3438–3455.
6. Simon A, Olah S, Molnar G, Szabadics J, Tamas G (2005) Gap-junctional coupling between neurogliaform cells and various interneuron types in the neocortex. J Neurosci 25: 6278–6285.
7. Cramer NP, Keller A (2006) Cortical control of a whisking central pattern generator. J Neurophysiol 96: 209–217.
8. Cramer NP, Li Y, Keller A (2007) The whisking rhythm generator: a novel mammalian network for the generation of movement. J Neurophysiol 97: 2148–2158.
9. Hattox AM, Priest CA, Keller A (2002) Functional circuitry involved in the regulation of whisker movements. Journal of Comparative Neurology 442: 266–276.
10. Moore JD, Deschenes M, Furuta T, Huber D, Smear MC, et al. (2013) Hierarchy of orofacial rhythms revealed through whisking and breathing. Nature 497: 205–210.
11. Kleinfeld D, Deschenes M, Wang F, Moore JD (2014) More than a rhythm of life: breathing as a binder of orofacial sensation. Nat Neurosci 17: 647–651.
12. Hattox AM, Li Y, Keller A (2003) Serotonin regulates rhythmic whisking. Neuron 39: 343–352.
13. Brons M, Kaper TJ, Rotstein HG (2008) Introduction to focus issue: Mixed mode oscillations: Experiment, computation, and analysis. Chaos 18: 015101.
14. Nguyen Q-T, Wessel R, Kleinfeld D (2004) Developmental regulation of active and passive membrane properties in rat vibrissa motoneurones. Journal of Physiology 556: 203–219.
15. Harish O, Golomb D (2010) Control of the firing patterns of vibrissa motoneurons by modulatory and phasic synaptic inputs: a modeling study. J Neurophysiol 103: 2684–2699.
16. Nguyen Q-T, Kleinfeld D (2005) Positive feedback in a brainstem tactile sensorimotor loop. Neuron 45: 1–11.
17. Manuel M, Iglesias C, Donnet M, Leroy F, Heckman CJ, et al. (2009) Fast Kinetics, high frequency oscillations and sub-primary firing range in adult mouse spinal motoneurons. J Neurosci 29: 11246–11256.
18. Turkin VV, O'Neill D, Jung R, Iarkov A, Hamm TM (2010) Characteristics and organization of discharge properties in rat hindlimb motoneurons. J Neurophysiol 104: 1549–1565.
19. Iglesias C, Meunier C, Manuel M, Timofeeva Y, Delestree N, et al. (2011) Mixed mode oscillations in spinal motoneurons arise from a low excitability state. J Neurosci 31: 5829–5840.
20. Golomb D, Donner K, Shacham L, Shlosberg D, Amitai Y, et al. (2007) Mechanisms of firing patterns in fast-spiking cortical interneurons. PLoS Comput Biol 3: e156.
21. Golomb D (1998) Models of neuronal transient synchrony during propagation of activity through neocortical circuitry. J Neurophysiol 79: 1–12.
22. Rinzel J, Ermentrout GB (1998) Analysis of neural excitability and oscillations. In: Koch C, Segev I, editors. Methods in Neuronal Modeling: From Ions to Networks. 2nd ed. Cambridge: MIT Press. pp. 251–291.
23. Ermentrout B, Wechselberger M (2009) Canards, Clusters, and Synchronization in a Weakly Coupled Interneuron Model. Siam Journal on Applied Dynamical Systems 8: 253–278.
24. Pikovsky A, Rosenblum M (2007) Synchronization. Scholarpedia 2: 1459.
25. Schneidman E, Freedman B, Segev I (1998) Ion channel stochasticity may be critical in determining the reliability and precision of spike timing. Neural Comput 10: 1679–1703.
26. Yarom Y, Hounsgaard J (2011) Voltage fluctuations in neurons: signal or noise? Physiol Rev 91: 917–929.
27. Terrell GR (1999) Mathematical Statistics: A Unified Introduction. New York: Springer.
28. Press WH, Teukolsky SA, Vetterling WT, Flannery BP (1992) Numerical recipes in C. New York, N.Y.: Cambridge University Press,.
29. Simony E, Bagdasarian K, Herfst L, Brecht M, Ahissar E, et al. (2010) Temporal and spatial characteristics of vibrissa responses to motor commands. J Neurosci 30: 8935–8952.
30. Golomb D, Hansel D (2000) The number of synaptic inputs and the synchrony of large, sparse neuronal networks. Neural Comput 12: 1095–1139.
31. Guckenheimer J, Holmes P (1983) Nonlinear Oscillations, Dynamical Systems, and Bifurcations of Vector Fields. New York: Springer-Verlag.
32. Wechselberger M (2005) Existence and bifurcation of canards in R-3 in the case of a folded node. Siam Journal on Applied Dynamical Systems 4: 101–139.
33. Wechselberger M (2007) Canard. Scholarpedia 2: 1356.
34. Llinas RR, Grace AA, Yarom Y (1991) In vitro neurons in mammalian cortical layer 4 exhibit intrinsic oscillatory activity in the 10- to 50-Hz frequency range. Proc Natl Acad Sci U S A 88: 897–901.
35. Gutfreund Y, Yarom Y, Segev I (1995) Subthreshold oscillations and resonant frequency in guinea-pig cortical neurons: physiology and modelling. J Physiol 483 (Pt 3): 621–640.
36. Alonso A, Llinas RR (1989) Subthreshold Na+-dependent theta-like rhythmicity in stellate cells of entorhinal cortex layer II. Nature 342: 175–177.
37. Alonso A, Klink R (1993) Differential electroresponsiveness of stellate and pyramidal-like cells of medial entorhinal cortex layer II. J Neurophysiol 70: 128–143.
38. Klink R, Alonso A (1993) Ionic mechanisms for the subthreshold oscillations and differential electroresponsiveness of medial entorhinal cortex layer II neurons. J Neurophysiol 70: 144–157.
39. Fransen E, Alonso AA, Dickson CT, Magistretti J, Hasselmo ME (2004) Ionic mechanisms in the generation of subthreshold oscillations and action potential clustering in entorhinal layer II stellate neurons. Hippocampus 14: 368–384.
40. Rotstein HG, Wechselberger M, Kopell N (2008) Canard Induced Mixed-Mode Oscillations in a Medial Entorhinal Cortex Layer II Stellate Cell Model. Siam Journal on Applied Dynamical Systems 7: 1582–1611.
41. Dorval AD Jr., White JA (2005) Channel noise is essential for perithreshold oscillations in entorhinal stellate neurons. J Neurosci 25: 10025–10028.
42. Dudman JT, Nolan MF (2009) Stochastically gating ion channels enable patterned spike firing through activity-dependent modulation of spike probability. PLoS Comput Biol 5: e1000290.
43. Dickson CT, Magistretti J, Shalinsky MH, Fransen E, Hasselmo ME, et al. (2000) Properties and role of I(h) in the pacing of subthreshold oscillations in entorhinal cortex layer II neurons. J Neurophysiol 83: 2562–2579.
44. Wang XJ (1993) Ionic basis for intrinsic 40 Hz neuronal oscillations. Neuroreport 5: 221–224.
45. Rubin J, Wechselberger M (2007) Giant squid-hidden canard: the 3D geometry of the Hodgkin-Huxley model. Biol Cybern 97: 5–32.
46. Pietr MD, Knutsen PM, Shore DI, Ahissar E, Vogel Z (2010) Cannabinoids reveal separate controls for whisking amplitude and timing in rats. J Neurophysiol 104: 2532–2542.
47. Hodgkin AL (1948) The local electric changes associated with repetitive action in a non-medullated axon. J Physiol (Lond) 107: 165–181.
48. Gao P, Bermejo R, Zeigler HP (2001) Whisker deafferentation and rodent whisking patterns: behavioral evidence for a central pattern generator. J Neurosci 21: 5374–5380.
49. Towal RB, Hartmann MJ (2006) Right-left asymmetries in the whisking behavior of rats anticipate head movements. J Neurosci 26: 8838–8846.
50. Grant RA, Sperber AL, Prescott TJ (2012) The role of orienting in vibrissal touch sensing. Front Behav Neurosci 6: 39.
51. Simony E, Ahissar E, Golomb D (2011) Sensory modulation of rhythmic whisking in response to contact. Soc Neurosc Abs 36: 76.10.
52. Prescott SA, Sejnowski TJ (2008) Spike-rate coding and spike-time coding are affected oppositely by different adaptation mechanisms. J Neurosci 28: 13649–13661.
53. Ermentrout B (2002) Simulating, analyzing, and animating dynamical systems: a guide to XPPAUT for researchers and students (software, environment, tools). Philadelphia: Society for Industrial and Applied Mathematics.